LETTERS

Exploring the thermodynamics of a universal Fermi gas

S. Nascimbène[1], N. Navon[1], K. J. Jiang[1], F. Chevy[1] & C. Salomon[1]

One of the greatest challenges in modern physics is to understand the behaviour of an ensemble of strongly interacting particles. A class of quantum many-body systems (such as neutron star matter and cold Fermi gases) share the same universal thermodynamic properties when interactions reach the maximum effective value allowed by quantum mechanics, the so-called unitary limit[1,2]. This makes it possible in principle to simulate some astrophysical phenomena inside the highly controlled environment of an atomic physics laboratory. Previous work on the thermodynamics of a two-component Fermi gas led to thermodynamic quantities averaged over the trap[3–5], making comparisons with many-body theories developed for uniform gases difficult. Here we develop a general experimental method that yields the equation of state of a uniform gas, as well as enabling a detailed comparison with existing theories[6–15]. The precision of our equation of state leads to new physical insights into the unitary gas. For the unpolarized gas, we show that the low-temperature thermodynamics of the strongly interacting normal phase is well described by Fermi liquid theory, and we localize the superfluid transition. For a spin-polarized system[16–18], our equation of state at zero temperature has a 2 per cent accuracy and extends work[19,20] on the phase diagram to a new regime of precision. We show in particular that, despite strong interactions, the normal phase behaves as a mixture of two ideal gases: a Fermi gas of bare majority atoms and a non-interacting gas of dressed quasi-particles, the fermionic polarons[10,18,20–22].

In this Letter we study the thermodynamics of a mixture of the two lowest spin states ($i = 1, 2$) of ^{6}Li prepared at a magnetic field $B = 834$ G (see Methods), where the dimensionless number $1/k_F a$ characterizing the s-wave interaction is equal to zero, the unitary limit. (Here k_F is the Fermi momentum and a the scattering length.) Understanding the universal thermodynamics at unitarity is a challenge for many-body theories because of the strong interactions between particles. Despite this complexity at the microscopic scale, all the macroscopic properties of an homogeneous system are encapsulated within a single equation of state (EOS), $P(\mu_1, \mu_2, T)$, that relates the pressure P of the gas to the chemical potentials μ_i of the species i and to the temperature T. In the unitary limit, this relationship can be expressed as[1]:

$$P(\mu_1, \mu_2, T) = P_1(\mu_1, T)\, h\left(\eta = \frac{\mu_2}{\mu_1}, \zeta = \exp\left(\frac{-\mu_1}{k_B T}\right)\right) \qquad (1)$$

where $P_1(\mu_1, T) = -k_B T \lambda_{dB}^{-3}(T) f_{5/2}(-\zeta^{-1})$ is the pressure of a single component non-interacting Fermi gas. Here k_B is the Boltzmann constant, $\lambda_{dB}(T)$ is the de Broglie wavelength and $f_{5/2}(z) = \sum_{n=1}^{\infty} z^n / n^{5/2}$. $h(\eta,\zeta)$ is a universal function which contains all the thermodynamic information of the unitary gas (Fig. 1). In cold atomic systems, the inhomogeneity due to the trapping potential makes the measurement of $h(\eta, \zeta)$ challenging. However, this inhomogeneity of the trap can be turned into an advantage, as shown in refs 20 and 23.

We directly probe the local pressure of the trapped gas using *in situ* images, following a recent proposal[23]. In the local density approximation, the gas is locally homogeneous with local chemical potentials:

$$\mu_i(\mathbf{r}) = \mu_i^0 - V(\mathbf{r}) \qquad (2)$$

here μ_i^0 is the chemical potential at the bottom of the trap for species i and $V(\mathbf{r})$ is the trapping potential. Then a simple formula relates the pressure P to the doubly-integrated density profiles[23]:

$$P(\mu_{1z}, \mu_{2z}, T) = \frac{m\omega_r^2}{2\pi}\left(\bar{n}_1(z) + \bar{n}_2(z)\right) \qquad (3)$$

where $\bar{n}_i(z) = \int n_i(x, y, z)\mathrm{d}x\mathrm{d}y$, n_i being the atomic density. ω_r and ω_z are respectively the transverse and axial angular frequency of a cylindrically symmetric trap (see Fig. 2), m is the ^{6}Li mass, and $\mu_{iz} = \mu_i(0, 0, z)$ is the local chemical potential along the z axis. From a single image, we thus measure the EOS, equation (1), along the parametric line $(\eta, \zeta) = (\mu_{2z}/\mu_{1z}, \exp(-\mu_{1z}/k_B T))$; see below.

The interest of this method is straightforward. First, one directly measures the EOS of the uniform gas. Second, each pixel row z_i gives a point $h(\eta(z_i), \zeta(z_i))$ whose signal to noise ratio is essentially given by that of $\bar{n}_1(z) + \bar{n}_2(z)$; typically one experimental run leads to $\sim$100 points with a signal to noise ratio between 3 and 10. With about 40 images one gets $\sim$4,000 points $h(\eta, \zeta)$, which after averaging provides a low-noise EOS of standard deviation $\sigma = 2\%$. In the following we illustrate the efficiency of our method on two important sectors of the parameter space (η, ζ) in Fig. 1: the balanced gas at finite temperature $(1, \zeta)$ and the zero-temperature imbalanced gas $(\eta, 0)$.

We first measure the EOS of the unpolarized unitary gas at finite temperature, $P(\mu_1, \mu_2, T) = P(\mu, T)$. The measurement of $h(1, \zeta)$ through the local pressure, equation (3), can be done provided one knows the temperature T of the cloud and its central chemical potential μ^0.

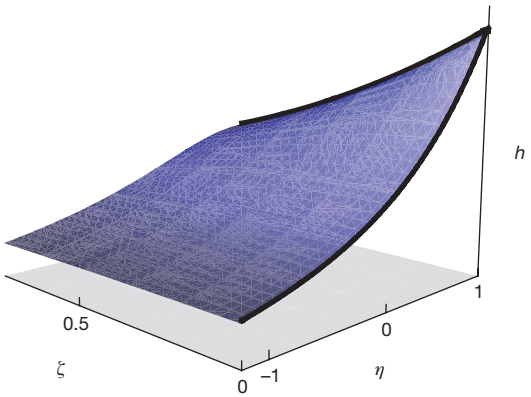

Figure 1 | Schematic representation of the universal function $h(\eta, \zeta)$. It fully describes the thermodynamics of the unitary gas as a function of chemical potential imbalance $\eta = \mu_2/\mu_1$ and of the inverse of the fugacity $\zeta = \exp(-\mu_1/k_B T)$. In this paper we measure the function h over the black lines $(1, \zeta)$ and $(\eta, 0)$, which correspond to the balanced unitary gas at finite temperature and to the spin-imbalanced gas at zero temperature, respectively.

[1]Laboratoire Kastler Brossel, CNRS, UPMC, École Normale Supérieure, 24 rue Lhomond, 75231 Paris, France.

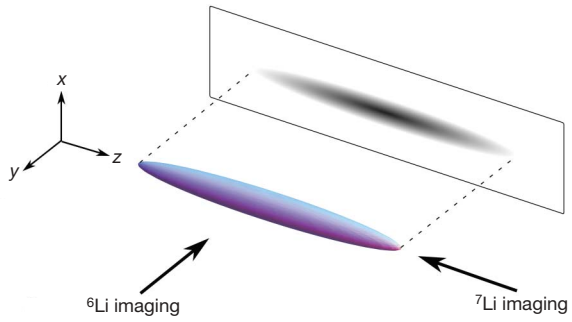

Figure 2 | Schematic representation of our atomic sample. The ^{6}Li atomic cloud is imaged in the direction y; the column density is then integrated along the direction x to give $\bar{n}(z)$. The ^{7}Li atoms are imaged after a time of flight along the z direction.

In the balanced case, model-independent thermometry is notoriously difficult because of the strong interactions. Inspired by ref. 24, we overcome this issue by measuring the temperature of a ^{7}Li cloud in thermal equilibrium with the ^{6}Li mixture (see Methods).

The central chemical potential μ^0 is fitted on the hottest clouds so that the EOS agrees in the classical regime $\zeta \gg 1$ with the second-order virial expansion $h(1, \zeta) \approx 2\left(1+\zeta^{-1}/\sqrt{2}\right)$ (ref. 25). For colder clouds we proceed recursively. The EOS of an image recorded at temperature T has some overlap with the previously determined EOS from all images with $T' > T$. In this overlap region, μ^0 is fitted to minimize the distance between the two EOSs. This provides a new portion of the EOS at lower temperature. Using 40 images of clouds prepared at different temperatures, we thus reconstruct a low-noise EOS from the classical part down to the degenerate regime, as shown in Fig. 3a.

We now comment on the main features of the EOS. At high temperature, the EOS can be expanded in powers of ζ^{-1} as a virial expansion[11]:

$$\frac{h(1,\zeta)}{2} = \frac{\sum_{k=1}^{\infty}\left((-1)^{k+1}k^{-5/2}+b_k\right)\zeta^{-k}}{\sum_{k=1}^{\infty}(-1)^{k+1}k^{-5/2}\zeta^{-k}}$$

where b_k is the k^{th} virial coefficient. As we have $b_2 = 1/\sqrt{2}$ in the measurement scheme described above, our data provide for the first time the experimental values of b_3 and b_4. $b_3 = -0.35(2)$ is in excellent agreement with the recent calculation $b_3 = -0.291 - 3^{-5/2} = -0.355$ from ref. 11, but not with $b_3 = 1.05$ from ref. 12. $b_4 = 0.096(15)$ involves the four-fermion problem at unitarity and could interestingly be computed along the lines of ref. 11.

Let us now focus on the low-temperature regime of the normal phase $\zeta \ll 1$. As shown in Fig. 3b, we observe a T^2 dependence of the pressure with temperature. This behaviour is reminiscent of a Fermi liquid, and indicates that pseudogap effects expected for strongly interacting Fermi superfluids[26] do not show up at the thermodynamic level within our experimental precision. In analogy with ^{3}He or heavy-fermion metals, we fit our data with the EOS:

$$P(\mu, T) = 2P_1(\mu, 0)\left(\xi_n^{-3/2} + \frac{5\pi^2}{8}\xi_n^{-1/2}\frac{m^*}{m}\left(\frac{k_B T}{\mu}\right)^2\right) \quad (4)$$

Here $P_1(\mu, 0) = 1/15\pi^2(2m/\hbar^2)^{3/2}\mu^{5/2}$ is the pressure of a single-component Fermi gas at zero temperature, m^* is the quasi-particle mass, and ξ_n^{-1} is the compressibility of the normal gas extrapolated to zero temperature, and normalized to that of an ideal gas of same density. We deduce two new parameters $m^*/m = 1.13(3)$ and $\xi_n = 0.51(2)$. Despite the strong interactions, m^* is close to m, unlike the weakly interacting ^{3}He liquid for which $2.7 < m^*/m < 5.8$, depending on pressure. Our ξ_n value is in agreement with the variational fixed-node Monte Carlo calculations $\xi_n = 0.54$ in ref. 27 and $\xi_n = 0.56$ in ref. 10, and with the quantum Monte Carlo calculation $\xi_n = 0.52$ in ref. 28. This yields the Landau parameters $F_0^s = \xi_n m^*/m - 1 = -0.42$ and $F_1^s = 3(m^*/m - 1) = 0.39$.

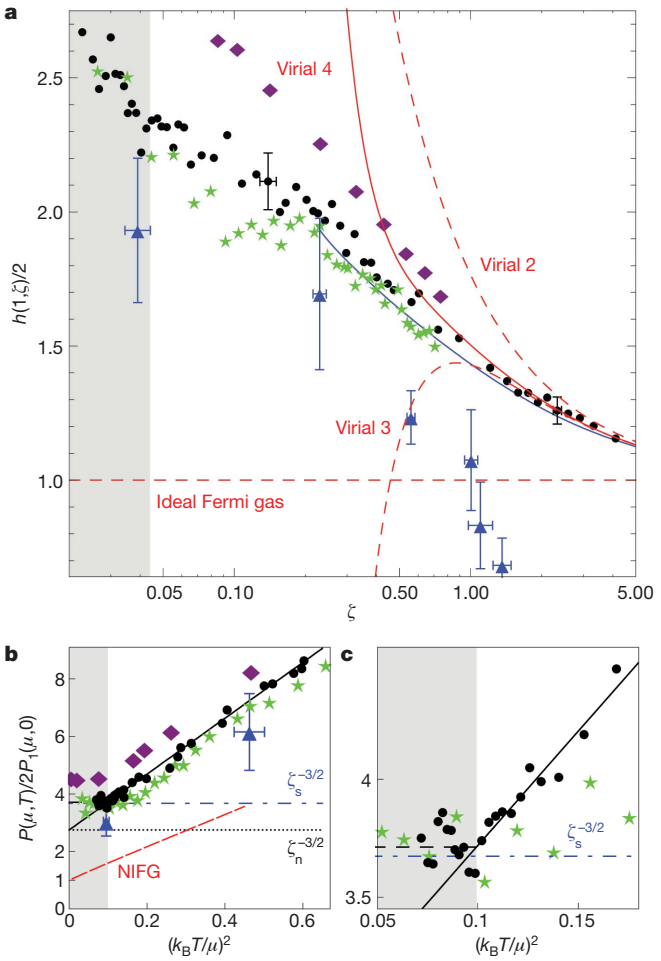

Figure 3 | Equation of state of a spin-balanced unitary Fermi gas. a, Finite-temperature equation of state (EOS) $h(1, \zeta)$ (black dots). The error bars represented at $\zeta = 0.14$ and $\zeta = 2.3$ indicate the 6% accuracy in ζ and h of our EOS. The red curves are the successive virial expansions up to fourth order. The blue triangles are from ref. 6, the green stars from ref. 7, the purple diamonds from ref. 8, and the blue solid line from ref. 9. The grey region indicates the superfluid phase. **b**, EOS $P(\mu, T)/2P_1(\mu, 0)$ as a function of $(k_BT/\mu)^2$, fitted by the Fermi liquid EOS, equation (4). The red dashed line is the non-interacting Fermi gas (NIFG). The horizontal dot-dashed and dotted lines indicate respectively the zero-temperature pressure of the superfluid phase $\propto \xi_s^{-3/2}$ and that of the normal phase $\propto \xi_n^{-3/2}$. **c**, Expanded view of **b** near T_c. The sudden deviation of the data from the fit occurs at $(k_BT/\mu)_c = 0.32(3)$ that we interpret as the superfluid transition. The black dashed line indicates the mean value of the data points below T_c.

In the lowest temperature points (Fig. 3c) we observe a sudden deviation of the data from the fitted equation (4) at $(k_BT/\mu)_c = 0.32(3)$ (see Supplementary Information). We interpret this behaviour as the transition from the normal phase to the superfluid phase. This critical ratio has been extensively calculated in recent years. Our value is in close agreement with the diagrammatic Monte Carlo calculation $(k_BT/\mu)_c = 0.32(2)$ of ref. 6 and with the quantum Monte Carlo calculation $(k_BT/\mu)_c = 0.35(3)$ of ref. 28; but it differs from the self-consistent approach in ref. 8 that gives $(k_BT/\mu)_c = 0.41$, from the renormalization group prediction 0.24 in ref. 29, and from several other less precise theories. From equation (4) we deduce the total density $n = n_1 + n_2 = \partial P(\mu_i = \mu, T)/\partial\mu$ and the Fermi energy $E_F = k_BT_F = \hbar^2/2m(3\pi^2 n)^{2/3}$ at the transition point. We obtain $(\mu/E_F)_c = 0.49(2)$ and $(T/T_F)_c = 0.157(15)$, in very good agreement with ref. 6. Our measurement is the first direct determination of $(\mu/E_F)_c$

and $(T/T_F)_c$ in the homogeneous gas. It agrees with the extrapolated value of the MIT measurement[19].

Below T_c, advanced theories[7,8] predict that $P(\mu, T)/2P_1(\mu, 0)$ is nearly constant (Fig. 3b). Therefore at $T = T_c$, $P/2P_1 \approx \xi_s^{-3/2} \approx 3.7$, and is consistent with our data. Here $\xi_s = 0.42(1)$ is the fundamental parameter characterizing the EOS of the balanced superfluid at zero temperature, a quantity extensively measured and computed in recent years[2].

Our data are compared at all temperatures with the calculations from refs 6–9 in Fig. 3a. The agreement with ref. 7 is very good for a large range of temperatures. Concerning ref. 6, the deviation from our data is about one error bar of the Monte Carlo method below $\zeta = 0.2$, and the deviation increases with temperature (Fig. 3a). Furthermore, we show in the Supplementary Information that $h(1, \zeta)/2$ must be greater than 1, an inequality violated by the two hottest Monte Carlo points of ref. 6.

From our homogeneous EOS we can deduce the EOS of the harmonically trapped unitary gas by integrating $h(1, \zeta)$ over the trap (see Supplementary Information). In particular, we find a critical temperature for the trapped gas $(T/T_F)_c = 0.19(2)$, where $T_F = \hbar\left(3\omega_r^2\omega_z N\right)^{1/3}$ and N is the total atom number. This value agrees very well with the recent measurement of ref. 30, and with less precise measurements[5,31,32].

Let us now explore a second line in the universal diagram $h(\eta, \zeta)$ (Fig. 1) by considering the case of the $T = 0$ spin-imbalanced mixture $\mu_2 \neq \mu_1$, that is, $\eta \neq 1$. Previous work[16–18] has shown that phase separation occurs in a trap. Below a critical population imbalance a fully paired superfluid occupies the centre of the trap. It is surrounded by a normal mixed phase and an outer rim consisting of an ideal gas of the majority component. In two out of the three previous experiments including ours[16,18], the local density approximation has been carefully checked. We are therefore justified in using equation (3) to analyse our data.

As in the previous case, the relationship between the pressure and the EOS requires the knowledge of the chemical potentials μ_1^0 and μ_2^0 at the centre of the trap. μ_1^0 is determined using the outer shell of the majority spin component ($i = 1$). The pressure profile $P(\mu_{1z}, \mu_{2z}, 0)$ corresponds to the Fermi–Dirac distribution and is fitted with the Thomas–Fermi formula $P_1 = \alpha\left(1 - z^2/R_1^2\right)^{5/2}$, providing $\mu_1^0 = \frac{1}{2} m\omega_z^2 R_1^2$. Using P_1 for the calculation of $h = P/P_1$ cancels many systematic effects on the absolute value of the pressure. Moreover, fitting the outer shell using a finite-temperature Thomas–Fermi profile[19], we measure a temperature $k_B T = 0.03(3)\mu_1^0$. μ_2^0 is fitted by comparison in the superfluid region with the superfluid EOS at zero temperature[21]:

$$h(\eta, 0) = (1+\eta)^{5/2} \Big/ (2\xi_s)^{3/2} \qquad (5)$$

Our measured EOS $h(\eta, 0)$ is displayed in Fig. 4. By construction our data agree for $\eta \gtrsim 0.1$ with equation (5). In Fig. 4 the slope of $h(\eta, 0)$ displays an obvious discontinuity for $\eta = \eta_c = 0.065(20)$. This is a signature of a first-order quantum phase transition to the partially polarized normal phase. The error bar is dominated by the uncertainty on ξ_s. This value is slightly higher than the prediction $\eta_c = 0.02$ given by the fixed-node Monte Carlo[10] and than the value $\eta_c = 0.03(2)$ measured in ref. 19.

From the relations $n_i = \partial P/\partial \mu_i$, we deduce from $h(\eta, 0)$ the density ratio n_2/n_1 (Fig. 4 inset). This ratio is discontinuous at the phase transition, from a maximum value in the normal phase $(n_2/n_1)_c = 0.5(1)$ to $n_2 = n_1$ in the superfluid phase. Our value is close to the zero-temperature calculation 0.44 (ref. 10) and agrees with the coldest MIT samples[19,20]. It confirms that the temperature is much smaller than the tricritical point temperature $T = 0.07T_F$ (ref. 19) where the discontinuity vanishes, justifying our $T = 0$ assumption made above.

For $\eta < \eta_c$ our data display a good agreement with a simple polaron model, based on the pioneering work in ref. 10. A polaron is a quasi-particle describing a single minority atom immersed in the majority Fermi sea[15,18,21,22]. It is characterized[10] by a renormalized

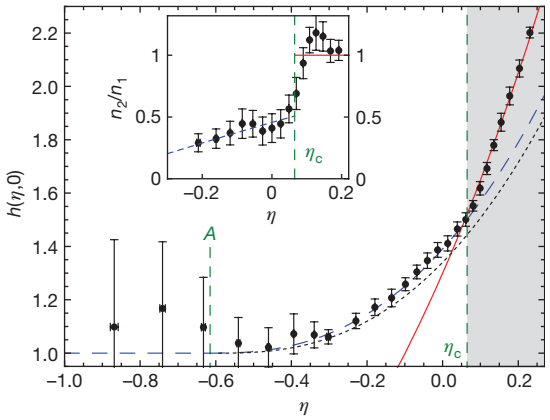

Figure 4 | Equation of state of the zero-temperature spin-imbalanced unitary gas $h(\eta, 0)$. The EOS is shown as filled black circles; error bars are equal to one standard error. The red solid line is the superfluid EOS, the blue dashed line is the ideal Fermi liquid, equation (7), with $A = -0.615$, $m^* = 1.20m$ and the black dotted line is the Monte Carlo calculation from ref. 10. Inset, local density ratio n_2/n_1 as a function of η. The red solid line $n_2/n_1 = 1$ corresponds to the fully paired superfluid and blue dashed line to the model, equation (7).

chemical potential $\mu_2 - A\mu_1$ and an effective mass m_p^*. Following this picture, we write the pressure as the sum of the Fermi pressures of ideal gases of majority atoms and of polarons:

$$P = \frac{1}{15\pi^2}\left(\frac{2m}{\hbar^2}\right)^{3/2}\left(\mu_1^{5/2} + \left(\frac{m_p^*}{m}\right)^{3/2}(\mu_2 - A\mu_1)^{5/2}\right) \qquad (6)$$

which can be written as:

$$h(\eta, 0) = 1 + \left(\frac{m_p^*}{m}\right)^{3/2}(\eta - A)^{5/2} \qquad (7)$$

A and m_p^* have recently been calculated exactly[14,15]: $A = -0.615$, $m_p^*/m = 1.20(2)$, and with these values inserted in equation (7) the agreement with our data is perfect. Note that our data lie slightly above the variational fixed-node Monte Carlo calculation[10]. We therefore conclude that interactions between polarons are not visible at this level of precision.

Alternatively, we can fit our data with m_p^*/m as a free parameter in equation (7). We obtain $m_p^*/m = 1.20(2)$. The uncertainty combines the standard error of the fit and the uncertainty on ξ_s. This value agrees with our previous measurement[18] $m_p^*/m = 1.17(10)$ (with a fivefold improvement in precision), with the theoretical value[14,15] $m_p^*/m = 1.20(2)$, and with the variational calculation[13]. It differs from the values 1.09(2) in ref. 33, 1.04(3) in ref. 10, and from the experimental value 1.06 in ref. 20.

We arrive at a simple physical picture of the $T = 0$ spin-polarized gas: the fully paired superfluid is described by an ideal gas EOS renormalized by a single coefficient ξ_s; the normal phase is nothing but two ideal gases, one of bare majority particles and one of polaronic quasiparticles.

In conclusion, we have introduced a powerful method for the measurement of the EOS of the unitary and homogeneous Fermi gas that enables direct comparison with theoretical models and provides a set of new parameters shown in Table 1. The method

Table 1 | Table of quantities measured in this work

Parameter	b_3	b_4	$(k_BT/\mu)_c$	$(\mu/E_F)_c$	$(T/T_F)_c$
Value	−0.35(2)	0.096(15)	0.32(3)	0.49(2)	0.157(15)
Parameter	ξ_n	m^*/m	η_c	$(n_2/n_1)_c$	m_p^*/m
Value	0.51(2)	1.13(3)	0.065(20)	0.5(1)	1.20(2)

can readily be extended to any multi-component cold atom gas in three dimensions that fulfils the local density approximation (see Supplementary Discussion). We have shown that the normal phase of the unitary Fermi gas is a strongly correlated system whose thermodynamic properties are well described by Fermi liquid theory, unlike high-T_c copper oxides.

Note added in proof: Since this paper was accepted for publication, we have become aware of the measurement of a similar equation of state for the balanced unitary Fermi gas at finite temperature by different methods[34].

METHODS SUMMARY

Our experimental set-up is presented elsewhere[18]. We load into an optical dipole trap and evaporate a mixture of ^{6}Li in the $|1/2, \pm 1/2\rangle$ states and of ^{7}Li in the $|1, 1\rangle$ state at 834 G. The cloud typically contains $N_6 = (5–10) \times 10^4$ atoms of ^{6}Li in each spin state and $N_7 = (3–20) \times 10^3$ atoms of ^{7}Li at a temperature from $T = 150$ nK to 1.3 μK. The ^{6}Li trap frequencies are $\omega_z/2\pi = 37$ Hz, $\omega_r/2\pi$ varying from 830 Hz to 2.20 kHz, and the trap depth is 25 μK for our hottest samples, with $T \approx 2T_F$. ^{6}Li atoms are imaged *in situ* using absorption imaging, while ^{7}Li atoms are imaged after time of flight, providing the temperature in the same experimental run (Fig. 4). As the scattering length describing the interaction between ^{7}Li and ^{6}Li atoms, $a_{67} = 2$ nm, is much smaller than k_F^{-1}, the ^{7}Li thermometer has no influence on the ^{6}Li density profiles. The ^{7}Li–^{6}Li collision rate, $\Gamma_{67} = 10\,s^{-1}$, is large enough to ensure thermal equilibrium between the two species.

Full Methods and any associated references are available in the online version of the paper at www.nature.com/nature.

Received 2 November 2009; accepted 6 January 2010.

1. Ho, T.-L. Universal thermodynamics of degenerate quantum gases in the unitarity limit. *Phys. Rev. Lett.* **92,** 090402 (2004).
2. Inguscio, M., Ketterle, W. & Salomon, C. (eds) *Proc. Int. School of Physics Enrico Fermi* (Course CLXIV, IOS Press, Amsterdam, 2006).
3. Stewart, J., Gaebler, J., Regal, C. & Jin, D. Potential energy of a ^{40}K Fermi gas in the BCS-BEC crossover. *Phys. Rev. Lett.* **97,** 220406 (2006).
4. Luo, L., Clancy, B., Joseph, J., Kinast, J. & Thomas, J. Measurement of the entropy and critical temperature of a strongly interacting Fermi gas. *Phys. Rev. Lett.* **98,** 080402 (2007).
5. Luo, L. & Thomas, J. Thermodynamic measurements in a strongly interacting Fermi gas. *J. Low Temp. Phys.* **154,** 1–29 (2009).
6. Burovski, E., Prokofev, N., Svistunov, B. & Troyer, M. Critical temperature and thermodynamics of attractive fermions at unitarity. *Phys. Rev. Lett.* **96,** 160402 (2006).
7. Bulgac, A., Drut, J. & Magierski, P. Spin 1/2 fermions in the unitary regime: a superfluid of a new type. *Phys. Rev. Lett.* **96,** 090404 (2006).
8. Haussmann, R., Rantner, W., Cerrito, S. & Zwerger, W. Thermodynamics of the BCS-BEC crossover. *Phys. Rev. A* **75,** 023610 (2007).
9. Combescot, R., Alzetto, F. & Leyronas, X. Particle distribution tail and related energy formula. *Phys. Rev. A* **79,** 053640 (2009).
10. Lobo, C., Recati, A., Giorgini, S. & Stringari, S. Normal state of a polarized Fermi gas at unitarity. *Phys. Rev. Lett.* **97,** 200403 (2006).
11. Liu, X., Hu, H. & Drummond, P. Virial expansion for a strongly correlated Fermi gas. *Phys. Rev. Lett.* **102,** 160401 (2009).
12. Rupak, G. Universality in a 2-component Fermi system at finite temperature. *Phys. Rev. Lett.* **98,** 090403 (2007).
13. Combescot, R., Recati, A., Lobo, C. & Chevy, F. Normal state of highly polarized Fermi gases: simple many-body approaches. *Phys. Rev. Lett.* **98,** 180402 (2007).
14. Combescot, R. & Giraud, S. Normal state of highly polarized Fermi gases: full many-body treatment. *Phys. Rev. Lett.* **101,** 050404 (2008).
15. Prokof'ev, N. & Svistunov, B. Fermi-polaron problem: diagrammatic Monte Carlo method for divergent sign-alternating series. *Phys. Rev. B* **77,** 020408 (2008).
16. Shin, Y., Zwierlein, M., Schunck, C., Schirotzek, A. & Ketterle, W. Observation of phase separation in a strongly interacting imbalanced Fermi gas. *Phys. Rev. Lett.* **97,** 030401 (2006).
17. Partridge, G., Li, W., Kamar, R., Liao, Y. & Hulet, R. Pairing and phase separation in a polarized Fermi gas. *Science* **311,** 503–505 (2006).
18. Nascimbene, S. *et al.* Collective oscillations of an imbalanced Fermi gas: axial compression modes and polaron effective mass. *Phys. Rev. Lett.* **103,** 170402 (2009).
19. Shin, Y., Schunck, C., Schirotzek, A. & Ketterle, W. Phase diagram of a two-component Fermi gas with resonant interactions. *Nature* **451,** 689–693 (2008).
20. Shin, Y. Determination of the equation of state of a polarized Fermi gas at unitarity. *Phys. Rev. A* **77,** 041603 (2008).
21. Chevy, F. Universal phase diagram of a strongly interacting Fermi gas with unbalanced spin populations. *Phys. Rev. A* **74,** 063628 (2006).
22. Schirotzek, A., Wu, C.-H., Sommer, A. & Zwierlein, M. W. Observation of Fermi polarons in a tunable Fermi liquid of ultracold atoms. *Phys. Rev. Lett.* **102,** 230402 (2009).
23. Ho, T.-L. & Zhou, Q. Obtaining phase diagram and thermodynamic quantities of bulk systems from the densities of trapped gases. *Nature Phys.* **6,** 131–134 (2010).
24. Spiegelhalder, F. *et al.* Collisional stability of ^{40}K immersed in a strongly interacting Fermi gas of ^{6}Li. *Phys. Rev. Lett.* **103,** 223203 (2009).
25. Ho, T.-L. & Mueller, E. High temperature expansion applied to fermions near Feshbach resonance. *Phys. Rev. Lett.* **92,** 160404 (2004).
26. Chen, Q., Stajic, J., Tan, S. & Levin, K. BCS BEC crossover: from high temperature superconductors to ultracold superfluids. *Phys. Rep.* **412,** 1–88 (2005).
27. Carlson, J., Chang, S., Pandharipande, V. & Schmidt, K. Superfluid Fermi gases with large scattering length. *Phys. Rev. Lett.* **91,** 050401 (2003).
28. Bulgac, A., Drut, J. & Magierski, P. Quantum Monte Carlo simulations of the BCS-BEC crossover at finite temperature. *Phys. Rev. A* **78,** 023625 (2008).
29. Gubbels, K. & Stoof, H. Renormalization group theory for the imbalanced Fermi gas. *Phys. Rev. Lett.* **100,** 140407 (2008).
30. Riedl, S., Guajardo, E., Kohstall, C., Denschlag, J. & Grimm, R. Superfluid quenching of the moment of inertia in a strongly interacting Fermi gas. Preprint at ⟨http://arXiv.org/abs/0907.3814⟩ (2009).
31. Greiner, M., Regal, C. & Jin, D. Emergence of a molecular Bose-Einstein condensate from a Fermi gas. *Nature* **426,** 537–540 (2003).
32. Inada, Y. *et al.* Critical temperature and condensate fraction of a fermion pair condensate. *Phys. Rev. Lett.* **101,** 180406 (2008).
33. Pilati, S. & Giorgini, S. Phase separation in a polarized Fermi gas at zero temperature. *Phys. Rev. Lett.* **100,** 030401 (2008).
34. Horikoshi, M., Nakajima, S., Ueda, M. & Mukaiyama, T. Measurement of universal thermodynamic functions for a unitary Fermi gas. *Science* **327,** 442–445 (2010).

Supplementary Information is linked to the online version of the paper at www.nature.com/nature.

Acknowledgements We are grateful to R. Combescot, X. Leyronas, Y. Castin, A. Recati, S. Stringari, S. Giorgini, M. Zwierlein and T. Giamarchi for discussions and to C. Cohen-Tannoudji, J. Dalibard, F. Gerbier and G. Shlyapnikov for critical reading of the manuscript. We acknowledge support from ESF (Euroquam), SCALA, ANR FABIOLA, Région Ile de France (IFRAF), ERC and Institut Universitaire de France.

Author Contributions S.N. and N.N. contributed equally to this work. S.N., N.N. and K.J.J. took the experimental data, and all authors contributed to the data analysis and writing of the manuscript.

Author Information Reprints and permissions information is available at www.nature.com/reprints. The authors declare no competing financial interests. Correspondence and requests for materials should be addressed to S.N. (sylvain.nascimbene@ens.fr).

METHODS

Construction of the EOS by successive patches. A typical image at high temperature provides about 100 pixels corresponding to ζ values varying from 2 at the trap centre to 6 at the edges, with a signal-to-noise from 3 to 10. Seven such images are fitted in the wings using the second-order virial expansion and averaged to obtain a low-noise EOS up to $\zeta = 2$. Then images of clouds where the evaporation has been pushed to a slightly lower temperature are recorded. They show about 75% overlap in ζ with the previous EOS. After minimization of the distance between a new image and the previously determined EOS in the overlap region, we obtain the value of μ^0 for a single image with 3% statistical uncertainty. This process is repeated for six successive trap depths. When averaging one image with typically 10 previous images, we obtain a new EOS with an error on ζ of about $0.03/\sqrt{10} \approx 1\%$. The EOS experiences a random walk error on the 40 images of $0.01 \times \sqrt{40} \approx 5\%$ for the coldest data. An independent check of the maximum error is provided by the good agreement with the superfluid EOS for temperatures lower than T_c (refs 7, 8).

Evaluation of the systematic uncertainties. For the measurement of $h(1, \zeta)$, the combined uncertainties on the radial frequency of the trap, trap anharmonicity, magnification of our imaging system, and atom counting affect the pressure measurement given in equation (3) at $\sim$20% level. However, two measurements, one at relatively high temperature and one at very low temperature, enable us to show that the overall error does not exceed 6%. In the temperature range $\zeta > 0.5$, the agreement between the experimental value $b_3 = -0.35(2)$ and the theoretical value $b_3 = -0.355$ of the third virial coefficient indicates that the global systematic error is smaller than 6%. Second, at very low temperature, theory[7,8] predicts that the variation of $P/2P_1$ as a function of $k_B T/\mu$ in the superfluid phase remains smaller than 5%. Our value of $P/2P_1 = 3.75$ below the critical point is within 5% of the $T = 0$ prediction $\xi_s^{-3/2} = 3.7(2)$. This confirms that systematic errors for our coldest samples are also smaller than 6%.

For the determination of the critical transition to superfluidity we fit the low-temperature data $P(\mu, T)/2P_1(\mu, 0)$ with a variable horizontal line for $T < T_c$ and with the Fermi-liquid equation (4) for $T > T_c$. The result of the fit is the dashed black line in Fig. 3c, which intersects equation (4) at $(k_B T/\mu)_c = 0.315(8)$. This statistical error is negligible compared to the error induced by the 6% systematic uncertainty discussed above, justifying our very simplified fit procedure. Indeed a 6% error on the pressure induces a 10% error on μ for images recorded in the vicinity of the critical temperature, leading to $(k_B T/\mu)_c = 0.32(3)$.

For the measurement of $h(\eta, 0)$, the fit of the fully polarized wings of the cloud serves as a pressure calibration for the rest of the cloud, cancelling many systematic effects.

In order to estimate temperature effects in the polarized gas, let us first remark that in the superfluid phase corrections scale as T^4 for the bosonic excitations and are exponentially suppressed by the gap for the fermionic ones[7]. So in our temperature range $k_B T = 0.03\mu_1^0$ their contributions will be very small. On the other hand, in the partially polarized normal phase, we expect a typical Fermi liquid T^2 scaling. In order to obtain an estimate of the error on the EOS, we develop the following simple model. In equation (6) which describes a mixture of zero-temperature ideal gases, we replace the Fermi pressures by the finite-temperature pressures of ideal gases (see equation (1)):

$$P(\mu_1, \mu_2, T) = P_1(\mu_1, T) + \left(\frac{m_p^*}{m}\right)^{3/2} P_1(\mu_2 - A\mu_1, T)$$

and run the analysis described in the main text. At $T = 0.05\mu_1^0$, the correction on h is less than 1%, half of our current error bar.

Limit of ^{7}Li thermometry. As the scattering length between the ^{7}Li atoms, $a_{77} = -3$ nm is negative, the ^{7}Li cloud becomes unstable when a BEC forms. This occurs at $T \approx 150$ nK with typically 3,500 atoms. Precise thermometry with lower atom numbers becomes difficult. For the measurement of the zero-temperature EOS of the imbalanced gas, we do not use ^{7}Li thermometry but rather the fit of the wings of the majority spin component.